Realistic evaluation of the Coulomb potential in spherical nuclei and a test of the traditional approach

L. Xayavong [*] and Y. Lim [†]
Department of Physics, Yonsei University, Seoul 03722, South Korea

(Received 6 March 2023; accepted 28 November 2023; published 15 December 2023)

A realistic evaluation of the Coulomb potential has been conducted for a few selected nuclei using available model-independent data for the charge density and the recent development of the Coulomb energy-density functional. Employing the Woods-Saxon potential as a nuclear component, we can quantify the differences in proton single-particle energies caused by deviations from the model-independent data of the uniform distribution, the two-parameter Fermi function, and the charge density obtained from a microscopic Hartree-Fock calculation using the effective Skyrme interaction. The obtained energy differences are generally small in magnitude, typically around 100 keV or less, given that the parameters of the charge density models are appropriately determined. However, considerably larger differences arise when the last occupied state is highly filled and, at the same time, has a small orbital angular momentum. A notable example of such nuclei is the sulfur isotopes ($Z = 16$). Unfortunately, the uniform distribution cannot be used to evaluate the Coulomb exchange term within a well-established method due to its lack of differentiability at the surface of a nucleus. Traditionally, the missing exchange term is corrected by excluding the contribution of the last proton to the direct term. Our investigation of this approach reveals that its effect simply introduces the factor $(Z - 1)/Z$ into the Coulomb direct term. For medium to heavy nuclei (typically beyond the *sd* shell), the resulting proton levels are 300–800 keV higher than those obtained with the exact Fock term. Conversely, the results for lighter nuclei tend to be the opposite, as the factor $(Z - 1)/Z$ decreases rapidly as the atomic number approaches 1. Hence, this traditional approach should be avoided for precise nuclear structure calculations based on Woods-Saxon radial wave functions, particularly for shell-model calculations of the isospin-symmetry breaking correction to β-decay rates for electroweak interaction studies [J. C. Hardy and I. S. Towner, Phys. Rev. C **102**, 045501 (2020), and references therein]. The present study also suggests that the Coulomb exchange term should be included within the Woods-Saxon potential, using the Slater approximation or beyond, along with a realistic model of charge density.

DOI: 10.1103/PhysRevC.108.064310

I. INTRODUCTION

The Coulomb repulsion between protons is the most well-known component of the nuclear Hamiltonian. Its action results in a large class of nuclear properties, including the deviation from the $N = Z$ line of the stability valley or the fission phenomenon which yields a clean-cut limitation to the nuclear size. It also affects specific properties of β, proton, and α radioactivities. As the main actor in the violation of isospin symmetry, the Coulomb interaction also plays a significant role in various nuclear structure phenomena. Notably, it induces isospin mixing in nuclear states,leads to displacement energy between members of isobaric multiplets, and contributes to isospin forbidden transitions [1–4]. Furthermore, the correction for isospin-symmetry breaking has become a critical factor in low-energy precision tests of the electroweak sector of the standard model via nuclear β decays [5–7]. As such, properly accounting for the Coulomb interaction in a microscopic model of nuclear structure is of paramount importance.

Within the independent-particle framework, the A-nucleon problem is simplified to A single-nucleon problems, which start with an effective nucleon-nucleon interaction [8,9] or an effective potential [10,11]. Therefore, the resulting nuclear wave function is simply an antisymmetric product of individual wave functions, also known as the Slater determinant. As is well known, this simplified model itself has limited applications. In principle, the self-consistent spherical Hartree-Fock (HF) mean field is only appropriate for closed-shell systems. On the other hand, the phenomenological approach is typically optimized for single-particle or single-hole states, such as the low-lying states of nuclei near a closed-shell core. Nevertheless, the independent-particle potential serves as the fundamental component of the complete nuclear Hamiltonian and, therefore, is crucial for the success of all nuclear many-body approaches. In certain specific applications, it becomes necessary to include the Coulomb contribution in the one-body component, particularly in the shell model where the valence spaces are too small to account for all significant configurations induced by the Coulomb interaction. For instance, the shell-model description of the superallowed

[*] xayavong.latsamy@yonsei.ac.kr
[†] ylim@yonsei.ac.kr

$0^+ \to 0^+$ Fermi β decay would not align with the predictions of the standard model, unless the harmonic oscillator basis is substituted with realistic Woods-Saxon (WS) radial wave functions that properly incorporate the Coulomb and nuclear isovector effects [12–14]. Interestingly, the correction for isospin-symmetry breaking in this weak semileptonic process is primarily dominated by the difference between the radial wave functions of the proton and neutron. In particular, the radial mismatch between the initial and final states is significantly amplified when the proton-rich mother nuclei are weakly bound. On the other hand, the self-consistent HF eigenfunctions, while more realistic in many aspects, may suffer from a number of potential deficiencies, as discussed in Ref. [14], making them unsuitable for the precise description of isospin-symmetry breaking. Additionally, the HF mean field is fundamentally incompatible with the parentage expansion shell-model formalism described in Ref. [12], due to the requirement of adjusting a free parameter to reproduce separation energies relative to excited states of intermediate nuclei.

Due to the high precision achieved in experimental studies of superallowed $0^+ \to 0^+$ Fermi β decay, the dominant source of uncertainties in the extracted V_{ud} element of the Cabibbo-Kobayashi-Maskawa (CKM) quark-mixing matrix currently arises due to the correction for isospin-symmetry breaking. As a result, there is a pressing need for further refinement of the WS potential, especially concerning the Coulomb term. This term is primarily responsible for the mismatch between the radial wave functions of protons and neutrons.

In nearly all calculations within the phenomenological WS potential [10,11,15–17], the Coulomb repulsion is accounted for using the approximation of a uniformly distributed charge sphere of radius R_C:

$$V_C(r) = (Z-1)e^2 \begin{cases} \frac{1}{r}, & r > R_C \\ \frac{1}{R_C}\left(\frac{3}{2} - \frac{r^2}{2R_C^2}\right), & \text{otherwise,} \end{cases} \quad (1)$$

where R_C is usually taken as $R_C = r_0(A-1)^{\frac{1}{3}}$ with $r_0 \approx 1.26$ fm [11]. Alternatively R_C can be extracted from the charge radius R_{ch} via [18]

$$R_C^2 = \frac{5}{3}R_{ch}^2 - \frac{5}{2}\sum_{i=1}^{3}\theta_i r_i^2 - \frac{5}{4}\left(\frac{\hbar}{mc}\right)^2 + \frac{5}{2}\frac{b^2}{A}, \quad (2)$$

where the nuclear oscillator length parameter is given by $b^2 \approx A^{\frac{1}{3}}$ fm^2. An improved parametrization of b^2 can be found in Ref. [19]. The last three terms on the right-hand side of Eq. (2) accounts for the internal structure of a proton, where $\sum_i \theta_i r_i^2 = 0.518$ fm^2 [20], Darwin-Foldy term ($\hbar/mc = 0.21$ fm), and center-of-mass (c.m.) motion, respectively. It is important to note that an additional modification was made in the construction of Eq. (1). Specifically, the contribution of the last proton was excluded, resulting in the potential in Eq. (1) being proportional to $Z-1$ instead of Z, as expected in classical electromagnetism. This exclusion of the last proton can also be interpreted as a correction for the missing Coulomb exchange potential in the uniform charge approximation.

The primary objective of this study is twofold: to examine the expression (1) and to explore alternative or more realistic approaches. The ultimate aim is to reduce or systematically quantify the uncertainty on V_{ud} stemming from the Coulomb term in the WS potential.

In general, the Coulomb potential can be derived from the two-body Coulomb interaction using the variational principle. Its direct part is a well-known functional of the charge density, while its exchange counterpart can be treated with high precision using a local density approximation [21,22]. Consequently, the Coulomb potential can be determined in a self-consistent manner by minimizing the total energy, as demonstrated in the HF theory [8]. Alternatively, it can be independently evaluated from the nuclear component using charge density data obtained from external sources.

In this study, we conduct a comprehensive investigation of Eq. (1) from various perspectives. We closely examine the foundation of this expression, the uniform charge distribution, within the framework of the phenomenological WS mean field, utilizing model-independent data obtained from electron scattering experiments [23,24]. We also explore the impact of the self-interaction correction method, which reduces the magnitude of the Coulomb direct term. This correction is then compared against realistic functionals derived using a local density approximation, with or without the correction for the effect of charge density gradient [21,22]. Additionally, we compare the results with an exact treatment of the Coulomb exchange term, making reasonable assumptions. Furthermore, we address the challenges associated with evaluating the Coulomb exchange term when assuming a uniform distribution or when utilizing model-independent data. To expand our investigation beyond the scope of expression (1), we consider two realistic models for the charge-density distribution: the two-parameter Fermi (2pF) function and the microscopic Skyrme-HF calculation. Our calculations encompass a wide variety of nuclei, covering a mass range from $A = 16$ to 209. This diverse set includes two $N = Z$ closed-shell nuclei (^{16}O and ^{40}Ca), two $N \neq Z$ closed-shell nuclei (^{48}Ca and ^{208}Pb), two closed-subshell nuclei (^{28}Si and ^{32}S), and four open-shell nuclei (^{58}Ni, ^{205}Tl, ^{206}Pb, and ^{209}Bi).

The paper is organized as follows. In Sec. II, the standard parametrization structure of the WS potential is described. Section III reviews the density functional forms of the Coulomb direct and exchange terms as employed in the self-consistent mean-field theory. Section IV outlines the selection of input charge densities and discusses their properties. In Sec. V, a comparative test of the Coulomb potential is conducted for various charge density models and functional forms. Lastly, the summary and conclusion are given in Sec. VI.

II. NUCLEAR POTENTIAL

In this work, we employ the phenomenological WS potential as the nuclear component of our independent-particle Hamiltonian. This potential follows a standard parametrization structure, comprising central, spin-orbit,

isospin-dependent, and Coulomb terms, namely,

$$V(r) = V_0 f_0(r) - V_s\left(\frac{r_s}{\hbar}\right)^2 \frac{1}{r}\frac{d}{dr} f_s(r)\,\langle \vec{l}\cdot\vec{\sigma}\rangle + V_{\rm sym}(r) + \left(\frac{1}{2} - t_z\right) V_C(r), \tag{3}$$

where t_z represents the isospin projection of the nucleon, following the convention of $t_z = \frac{1}{2}$ for neutrons and $-\frac{1}{2}$ for protons. The functions $f_i(r)$ are defined as

$$f_i(r) = \frac{1}{1 + \exp\left(\frac{r - R_i}{a_i}\right)}, \tag{4}$$

where $i = 0$ or s denote either the central or spin-orbit terms. The restriction of $a_0 = a_s$ is commonly adopted due to a lack of experimental constraints. However, contrary to this assumption, a smaller spin-orbit radius ($R_s < R_0$) has been suggested, as the two-body spin-orbit interaction has a shorter range [17]. For example, the Seminole parametrization provided in Ref. [11] obtained $R_s/R_0 = 0.921$ as a more suitable value.

The expectation value $\langle \vec{l}\cdot\vec{\sigma}\rangle$ appearing in the spin-orbit term can be written as

$$\langle \vec{l}\cdot\vec{\sigma}\rangle = \begin{cases} l & \text{if} \quad j = l + \frac{1}{2} \\ -(l+1) & \text{if} \quad j = l - \frac{1}{2}. \end{cases} \tag{5}$$

In order to preserve the fundamental symmetries, phenomenological effective potentials such as WS are typically treated as nuclear mean fields created by the core of $(A-1)$ nucleons. The exclusion of the last nucleon's contribution also serves as a self-interaction correction due to the absence of exchange terms, as discussed for the Coulomb potential in the introduction. For these reasons, the WS radii are usually parametrized as a function of $(A-1)$ instead of A, namely $R_i = r_i(A-1)^{\frac{1}{3}}$. Furthermore, if we neglect the internal structure of the core of $(A-1)$ nucleons, the nucleus can be regarded as a system of two point-like particles. Within this simplified picture, the c.m. correction for the WS Hamiltonian can be easily implemented by replacing the nucleon mass m in the kinetic energy term of the radial Schrödinger's equation with the reduced mass μ, defined as

$$\mu = m\frac{(A-1)}{A}. \tag{6}$$

This c.m. correction is fully validated at large separations, where the contribution of the core structure is negligible. A further discussion of the c.m. corrections is given in Refs. [14,25].

Most nuclei have a different number of protons and neutrons. Apart from the Coulomb repulsion, the difference in the number of neutrons and protons in nuclei causes an additional shift in the potential depth between neutrons and protons. As experimental evidence, nuclei with $N = Z$ tend to have the greatest binding energy compared to other configurations of protons and neutrons. In practice, this effect is commonly accounted for by adding the symmetry term expressed as

$$V_{\rm sym}(r) = 2t_z V_1 \frac{(N-Z)}{A} f_0(r). \tag{7}$$

In this work, we simplify our analysis by neglecting the contribution of the symmetry term to the spin-orbit coupling [26]. It is important to note that some additional terms or slightly different parametrization structures can also be found in the literature. For example, a more fundamental form of the isospin-dependent term was proposed by Lane in Ref. [27]. However, the investigation of such variations in the nuclear component is beyond the scope of this work.

The Coulomb potential $V_C(r)$ can be evaluated using various methods, which will be described separately in the following sections.

The WS potential is not suitable for calculating the total binding energy, as it is not based on a specific effective two-body interaction. Typically, the WS parameters (V_0, V_s, r_0, r_s, a_0, a_s, V_1, R_C) are determined through a best fit of nuclear single-particle energies and charge radii. For this study, we will use the set of WS parameter values named BM$_m$, which is listed in Table I of Ref. [13].

III. COULOMB POTENTIAL AS A CHARGE DENSITY FUNCTIONAL

Before delving into the specifics of our study, it is essential to describe the fundamental formulas and general properties of the Coulomb potential in this section. According to the self-consistent HF theory [8], the Coulomb contribution to the mean field consists of a direct and an exchange term, which can be symbolically written as

$$V_C(r) = V_{\rm dir}(r) + V_{\rm exc}(r). \tag{8}$$

Throughout this paper, we assume spherical symmetry. The Coulomb direct term for a spherically symmetric nucleus, after integrating out the angular variables, is reduced to

$$V_{\rm dir}(r) = 4\pi e^2\left[\frac{1}{r}\int_0^r x^2\rho_{ch}(x)\,dx + \int_r^\infty x\rho_{ch}(x)\,dx\right]. \tag{9}$$

One can observe here that if the charge density $\rho_{ch}(r)$ is constant inside the radius R_C and vanishes elsewhere, the expression (9) will return the potential in Eq. (1) except that it would be proportional to Z instead of $Z-1$ as explained in the introduction. Further details on the uniform charge distribution are given in Sec. IV B.

Since the Coulomb force has an infinite range, the Coulomb exchange term becomes nonlocal in coordinate space, posing a challenge for its calculation, particularly within the self-consistent mean-field framework. To circumvent this issue, a common approach is to use a local density approximation. One widely used approximation is the one proposed by Slater [22], in which the Coulomb exchange term is expressed as a function of the charge density

$$V_{\rm exc}^{\rm Sla}(r) = -e^2\left[\frac{3}{\pi}\rho_{ch}(r)\right]^{\frac{1}{3}}. \tag{10}$$

The accuracy of this approximation was tested against exact calculations [28] for various spherical nuclei ranging from ^{16}O to $^{310}_{126}$Ubh. The proton energy levels obtained using the Slater approximation were found to be underbound by 100 to 550 keV for occupied states and overbound by 100 to 200 keV

for unoccupied states, compared with those obtained using the exact Fock term.

Recently, it was demonstrated that the Coulomb energy density functional built using the generalized gradient approximation (GGA) [21] achieves nearly the same level of accuracy for the total energy as the exact treatment of the Fock term, while maintaining the same numerical efficiency as the Slater approximation. The Coulomb exchange term derived from the GGA depends not only on the charge density but also on its gradient with respect to radial distance. The GGA-exchange term is given by

$$V_{\rm exc}^{GGA}(r) = V_{\rm exc}^{\rm Sla}(r)\Bigg\{F(s) - \left[s + \frac{3}{4k_F r}\right]F'(s) + \left[s^2 - \frac{3\rho''_{ch}(r)}{8\rho_{ch}(r)k_F^2}\right]F''(s)\Bigg\}, \tag{11}$$

where $\rho''_{ch}(r)$ denotes the second derivative of $\rho_{ch}(r)$ with respect to r, and $F'(s)$ and $F''(s)$ represents the first and second derivatives of $F(s)$ with respect to s, respectively. Note that $F(s)$ is the enhancement factor introduced for the Coulomb exchange potential in GGA. Following Perdew-Burke-Ernzerhof [29], $F(s)$ is parametrized as

$$F(s) = 1 + \kappa - \frac{\kappa}{1 + \mu s^2/\kappa}, \tag{12}$$

where the two parameters κ and μ have been recently revised for nuclear physics applications by Naito *et al.* [21] and the best-fit values were determined to be 0.804 and 0.274, respectively. The function s represents the dimensionless density gradient defined as

$$s = \frac{|\nabla\rho_{ch}(r)|}{2k_F\rho_{ch}(r)}, \tag{13}$$

where $|\nabla\rho_{ch}(r)|$ is the norm of $\nabla\rho_{ch}(r)$, and the Fermi momentum is given by $k_F = [3\pi^2\rho_{ch}(r)]^{\frac{1}{3}}$. It is worth noting that if $\rho_{ch}(r)$ is a slowly varying function of r, its gradient will vanish ($s = 0$), and therefore $F(0) = 1$, then the Coulomb exchange term in Eq. (11) will be reduced to the Slater approximation (10). Considering the overall behavior of charge density in a nucleus, the Coulomb exchange potential from the GGA is mostly affected in the nuclear surface region, where the charge density gradient is peaked.

The contribution of higher-order electromagnetic effects, such as vacuum polarization and Coulomb spin-orbit can also be included. However, both of them were found to be completely negligible [14].

IV. INPUT CHARGE DENSITIES

According to the formalism reviewed in the previous section, the charge density serves as the fundamental ingredient for determining the Coulomb potential. In the following list, we provide a brief description of the conventional methods used to deduce charge density from electron scattering, also known as model-independent analyses. The data obtained from this source is used as a reference for our comparative study. Additionally, we discuss frequently used hypothetical and phenomenological models, as well as the microscopic self-consistent mean-field calculation of the charge density. The validity of these theoretical models as input for the Coulomb potential is further investigated in the next section.

A. Model-independent analyses

The charge form factors for several stable nuclei have been accurately measured through electron scattering. These data are commonly analyzed using two model-independent approaches to obtain numerical values for the charge density as a function of r. The first approach is the Fourier-Bessel (FB) expansion [30], and the second is the sum-of-Gaussians (SOG) expansion [24]. In the FB approach, the charge density is expanded in terms of the spherical Bessel function of order zero (j_0), given by

$$\rho_{\rm FB}(r) = \begin{cases} \sum_{\nu=1}^{n_{\rm max}} a_\nu j_0\left(\frac{\nu\pi r}{R_{\rm cut}}\right), & r \leqslant R_{\rm cut} \\ 0, & \text{otherwise,} \end{cases} \tag{14}$$

where a_ν are the expansion coefficients and $R_{\rm cut}$ is a cut-off radius beyond which the charge density is sufficiently small and is equated to zero. The first $n_{\rm max}$ coefficients of this series expansion are obtained directly from the experimental data [23]. Here, $n_{\rm max} = R_{\rm cut}q_{\rm max}/\pi$, where $q_{\rm max}$ is the maximum momentum transfer up to which the charge form factor data are determined. For the normalization, the integral of $\rho_{\rm FB}(r)$ over all spaces must be equal to the total nuclear charge $+Ze$.

In the SOG approach, the charge density is expressed as

$$\rho_{\rm SOG}(r) = \sum_{i=1}^{m_{\rm max}} A_i\{\exp[-x_i(r)^2] + \exp[-y_i(r)^2]\}, \tag{15}$$

where $y_i(r) = (r + R_i)/\gamma$ and $x_i(r) = (r - R_i)/\gamma$. The expansion coefficients A_i are given by

$$A_i = \frac{ZeQ_i}{2\pi^{\frac{3}{2}}\gamma^3\left(1 + 2R_i^2/\gamma^2\right)}, \tag{16}$$

where γ is the width of the Gaussians and is related to the root-mean-square (rms) radius through $R_g = \gamma\sqrt{3/2}$. According to Sick [24], γ is chosen equal to the smallest width of the peaks in the nuclear radial wave functions calculated using the HF method. The author reported that the γ values extracted from the harmonic oscillator and WS radial wave functions yield almost identical results. The charge fraction Q_i must be normalized such that $\sum_i Q_i = 1$.

In practice, a few terms are included within the sum in Eqs. (14) and (15). For example, a truncation with $n_{\rm max} \leqslant 17$ and $m_{\rm max} \leqslant 12$ was imposed for the analyses carried out in Ref. [23]. The parameters of $\rho_{\rm FB}(r)$ and $\rho_{\rm SOG}(r)$ deduced from experiments are given in the data compilation [23].

We note that the charge density obtained from the FB approach exhibits an undesirable property—it contains an oscillatory component and, in some cases, even acquires negative values near the cut-off radius $R_{\rm cut}$, as illustrated in the right panel of Fig. 1. Although these oscillations are of extremely small magnitude, they can be greatly amplified by the first and second derivatives, leading to significant errors when the GGA is employed to calculate the Coulomb exchange term. On the other hand, oscillations in the asymptotics of

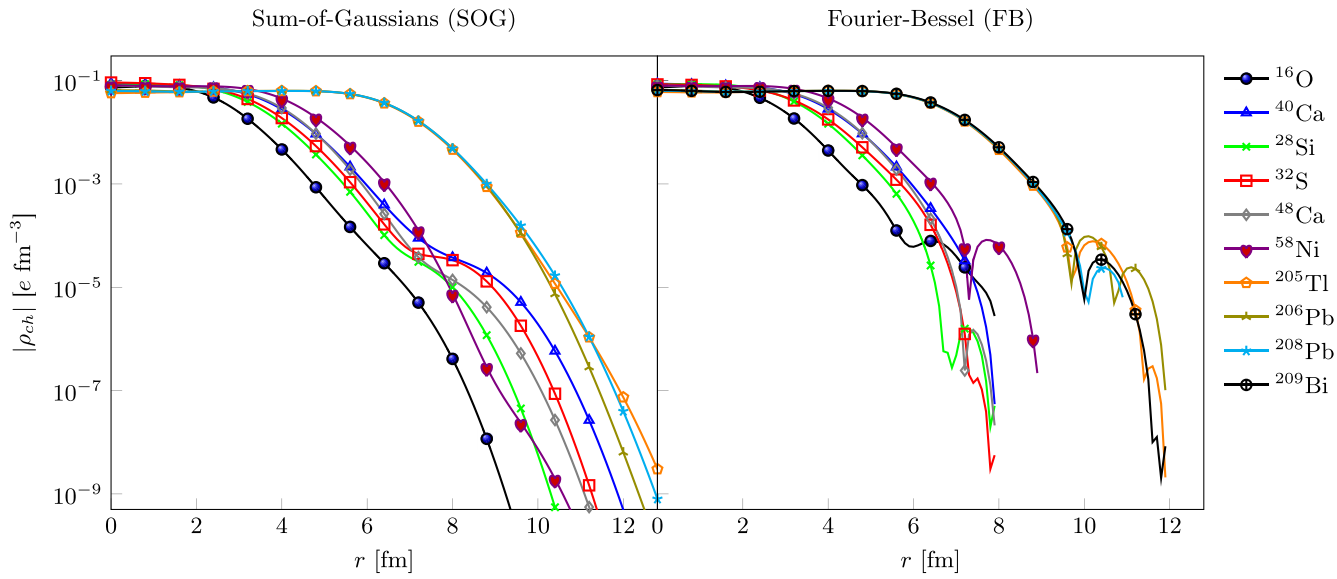

FIG. 1. Illustration of oscillations in the charge densities deduced from electron scattering experiments using the FB (right) and SOG (left) analyses [23].

the charge density obtained from the SOG approach are also visible for some nuclei, but their magnitude is generally much smaller (with a larger width), as shown in the left panel of Fig. 1. This unphysical property arises from the incompleteness of the expansions and the use of a cut-off radius that is too small in the FB analysis. In reality, the tail of the charge density should decrease monotonically since the asymptotic radial wave functions decay exponentially.

In order to avoid this problem, we replace both FB and SOG data from a point just before the oscillations occur (denoted as R_x) towards infinity with the 2pF function (see Sec. IV C for the definition of 2pF). For both data sets, we select $R_x = 4.5$ fm for nuclei with $A \leqslant 58$ and $R_x = 8.5$ fm for heavier nuclei. Instead of performing a global fit, we determine the parameters of the 2pF function by matching it, as well as its first and second derivatives, with those of the data at R_x. The resulting 2pF function might not be optimal for the entire range of available data in the domain of $[R_x, +\infty]$; however, this approach ensures the continuity of the charge density at R_x. It is important to note that this replacement does not introduce a significant error since the charge density in this domain is small. By employing this technique, we overcome the unphysical oscillations present in the original FB and SOG data, obtaining a smooth charge density representation for further calculations.

B. Uniform charge distribution

For a sphere of radius R_C containing a total charge of $+Ze$ uniformly distributed throughout its volume, the charge density is given by

$$\rho_{\text{Unif}}(r) = \begin{cases} \rho_0, & r \leqslant R_C \\ 0, & \text{otherwise}, \end{cases} \tag{17}$$

and the normalization condition implies that

$$\rho_0 = \frac{3Ze}{4\pi R_C^3}. \tag{18}$$

In this work, we follow the approach in Ref. [31], where $\rho_{\text{Unif}}(r)$ is considered as a pointed proton distribution and is normalized to Z instead of $+Ze$. Therefore, its rms radius (denoted as R_{Unif}) can be calculated analytically as

$$R_{\text{Unif}} = R_C\sqrt{\frac{3}{5}}. \tag{19}$$

In this uniform distribution, corrections for finite size, Darwin-Foldy term, and c.m. motion must be introduced in order to convert R_{Unif} into the charge radius. Equation (19) provides an experimental constraint for R_C, at least for the cases where the experimental data are available. Otherwise, it can be parameterized as usual, namely $R_C = r_C(A-1)^{\frac{1}{3}}$ where $r_C \approx 1.26$ fm [11]. The validity of various methods for determining R_C can also be tested within the framework of the present study. Further discussions on this point are given in the next section.

Because of its simplicity, the uniform charge distribution is widely used in nuclear physics, particularly in the context of the nuclear optical model. However, it should be noted that it is an assumption of classical electromagnetism and does not have quantum mechanical equivalent. This is because wave functions, which are the building blocks of charge density, must be continuous in coordinate space. Furthermore, the two aforementioned approaches to the Coulomb exchange term (Slater and GGA) are evidently inapplicable for this distribution due to its discontinuity and lack of differentiability at the surface of a nucleus.

C. Two-parameter Fermi function

We also consider a realistic phenomenological model for the charge density distribution, namely the two-parameter Fermi function,

$$\rho_{2pF}(r) = \frac{\tilde{\rho}_0}{1 + \exp\left(\frac{r-c}{z}\right)}. \tag{20}$$

Unlike the previous models, the 2pF is continuous and differentiable. Moreover, it decays monotonically towards large distances. Although, the 2pF function may appear similar to the $f_i(r)$ functions of the WS potential in Eq. (4), in general, the parameters c and z are smaller than the length and surface diffuseness parameters of the WS potential. It is also evident from the Skyrme HF theory that the mean field potential is not a linear function of densities. Thus, their geometrical characterizing parameters do not necessarily have to be the same as the WS potential parameters. More details on this point are given in Ref. [32].

As its name indicates, the 2pF is determined by two parameters because $\tilde{\rho}_0$ is obtained via the normalization condition,

$$\tilde{\rho}_0 = \frac{Ze}{4\pi z^3 F_2(c/z)}, \tag{21}$$

where $F_2(c/z)$ is the second-order Fermi integral (see Appendix C of Ref. [18]). Similar to the previous subsection, we employ the convention that $\rho_{2pF}(r)$ is normalized to Z. Therefore, the parameter c can be extracted from the charge radius by solving the following equation [18]:

$$R_{ch}^2 = \frac{4\pi\tilde{\rho}_0 z^5}{Z} F_4\left(\frac{c}{z}\right) + \frac{3}{2}\sum_{i=1}^{3}\theta_i r_i^2 + \frac{3}{4}\left(\frac{\hbar}{mc}\right)^2 - \frac{3}{2}\frac{b^2}{A}. \tag{22}$$

As before, the last three terms account for the finite size of the proton, the Darwin-Foldy term, and the c.m. motion, respectively. $F_4(c/z)$ is the fourth-order Fermi integral (see Appendix C of Ref. [18]).

Recently, Horiuchi [33] proposed a new method for determining the surface thickness of charge density. Implementing the Taylor expansion of $\rho_{2pF}(r)$ at $r = c$ and retaining up to the first-order term, the following relation was derived:

$$z = -\frac{\tilde{\rho}_0}{4}[\rho'_{2pF}(c)]^{-1}, \tag{23}$$

where $\rho'_{2pF}(c)$ denotes the first derivative of $\rho_{2pF}(r)$ at $r = c$. By matching ρ_{2pF} on the right-hand side of Eq. (23) with the charge density constructed from eigenfunctions of the WS potential whose Coulomb term is, in turn, a function of ρ_{2pF}, Eq. (23) can be solved in a self-consistent manner. This offers an alternative means for constraining z in the case where experimental data are not available.

Although this distribution nicely represents the diffuseness at the nuclear surface region, it is unable to describe the oscillations of the charge density observed in the nucleus interior. It has been shown that this difficulty can be overcome by extending Eq. (20) to the three-parameter Fermi (3pF) function [34]. However, the 3pF is not a good choice for a general application due to the lack of experimental data to constrain the third parameter.

D. Hartree-Fock calculations

Within a microscopic nuclear structure model, the charge density is essentially decomposed into three components:

$$\rho_{ch}(r) = \rho_{ch}^p(r) + \rho_{ch}^n(r) + \rho_{ch}^{ls}(r), \tag{24}$$

where $\rho_{ch}^p(r)/\rho_{ch}^n(r)$ comes from the finite charge distribution of the proton/neutron folded with the point-like proton/neutron density. Additionally, $\rho_{ch}^{ls}(r)$ represents the relativistic electromagnetic correction that depends on the spin-orbit coupling. However, the shape of the charge density distribution is primarily determined by the shape of the point-like proton density. The contributions $\rho_{ch}^n(r)$ and $\rho_{ch}^{ls}(r)$ were found to be negligibly small [14]. Furthermore, they tend to cancel each other out, so they will not be considered here.

By definition $\rho_{ch}^p(r)$ is given by

$$\rho_{ch}^p(r) = \int d\boldsymbol{r}'\rho_p(r')G_p(\boldsymbol{r} - \boldsymbol{r}'), \tag{25}$$

where $\boldsymbol{r}$ is the position vector in $\mathbb{R}^3$. The effective electromagnetic form factor G_p is taken as a sum of three Gaussians as described in Ref. [20]. The point-like proton density $\rho_p(r)$ can be defined in terms of proton radial wave functions $R_\alpha(r)$, namely,

$$\rho_p(r) = \frac{1}{4\pi}\sum_\alpha n_\alpha |R_\alpha(r)|^2, \tag{26}$$

where α stands for the spherical quantum numbers nlj and the sum is taken over over all occupied states. The proton occupation number n_α is obtained with the so-called equal-filling approximation. Therefore, for a closed-shell configuration, $n_\alpha = (2j + 1)$ for the occupied orbits and 0 for the unoccupied orbits.

The radial wave functions $R_\alpha(r)$ are obtained as the eigenfunctions of the Skyrme-HF mean field. We utilize the SLY5 parameter set [35] for the Skyrme Hamiltonian, which is invariant under rotation in the isospin space. For treating the Coulomb exchange term, we employ the Slater approximation. To simplify the analysis, we neglect the charge-symmetry and charge-independence breaking forces [36]. The HFBRAD program [9] is employed to solve the spherical Skyrme-HF equation, and we calculate the Coulomb terms using a point-like proton density. To account for the finite size effect, we apply Eq. (25) within an external program after the HF variation has terminated.

It should be noted that this HF calculation is used solely as an alternative model for the charge density, specifically for evaluating the Coulomb terms of the WS potential. No further self-consistent calculations are conducted in the present study.

V. COMPARATIVE STUDY OF COULOMB POTENTIAL

As a reminder, the Coulomb potential can be expressed as a functional of the charge density within a local density approximation. In Eq. (1), this behavior is also evident, with the charge density specified as the uniform charge distribution. Without self-consistency, the charge density and the functional can be considered as separate entities, each serving as a fundamental building block for the Coulomb potential.

Therefore, it is more appropriate to assess the quality of each individual entity separately, rather than evaluating the Coulomb potential within a given approach as a whole. This section begins by examining the uncertainties in the experimental charge density data and their impact on proton energy levels. The next step involves checking the charge density models listed in Sec. IV against the model-independent data by studying the proton single-particle energies. Finally, various approaches to the Coulomb functional, including Eq. (1) and those reviewed in Sec. III, will be tested against a realistic functional or an exact treatment based on existing calculations carried out within the Skyrme-HF framework [28,37].

A. Inspection of experimental charge density data

Before conducting a comparative study of the Coulomb potential, it is crucial to assess the influence of differences between the FB and SOG data for charge density on proton single-particle energies. For simplicity, we will neglect the uncertainties on the coefficients of the FB and SOG expansions, even though they are available from the data compilations. It is important to note that the focus of this section is on the proton single-particle energies. Other observables, such as the rms radii and neutron skin thicknesses, were found to be much less sensitive to small variations in the Coulomb terms.

Furthermore, instead of conducting a point-by-point comparison, we introduce the following radial mismatch factor, denoted as Λ, as an effective measure for the charge density differences:

$$\Lambda = \frac{\bar{\Omega} - \Omega}{\bar{\Omega}}, \tag{27}$$

where Ω represents the overlap integral between the FB and SOG data,

$$\Omega = 4\pi \int_0^\infty \rho_{\rm FB}(r)\rho_{\rm SOG}(r) r^2 dr. \tag{28}$$

Meanwhile, $\bar{\Omega}$ corresponds to the integral of their average squared:

$$\bar{\Omega} = 4\pi \int_0^\infty \left[\frac{\rho_{\rm FB}(r) + \rho_{\rm SOG}(r)}{2}\right]^2 r^2 dr. \tag{29}$$

The resulting Λ values in % are as follows: 3.441×10^{-3} (^{16}O), 5.659×10^{-3} (^{28}Si), 0.209 (^{32}S), 2.601×10^{-2} (^{40}Ca), 4.126×10^{-2} (^{48}Ca), 3.866×10^{-3} (^{58}Ni), 3.641×10^{-4} (^{205}Tl), 5.048×10^{-4} (^{206}Pb), and 1.459×10^{-2} (^{208}Pb).

We recall that the exact Coulomb exchange term is nonlocal in coordinate space and cannot be expressed as a function of charge density. Therefore, it is not suitable for the present study, where the self-consistent HF mean field is replaced with the phenomenological WS potential. To investigate whether the choice of the Coulomb exchange functional influences the impact of the FB-SOG charge density differences on proton single-particle energies, we consider three different approximations for the Coulomb potential. One of them consists purely of the direct term, while the other two include an exchange term employing either the Slater approximation or the GGA. By combining these approximations with the nuclear component described in Eq. (3), we obtain the single-particle energies and wave functions by solving the radial Schrödinger's equation. The splits in proton energies due to the differences in the charge density data are listed in Table I. A negative sign indicates that the FB data yield a lower proton energy level relative to that yielded by the SOG data, i.e., $\Delta E^{\rm FB}_{\rm SOG} = E_{\rm FB} - E_{\rm SOG}$. Conversely, a positive sign indicates the opposite. For completeness, the averaged proton energies between the FB and SOG results calculated using the GGA functional [denoted as $\bar{E}^{\rm FB}_{\rm SOG} = (E_{\rm FB} + E_{\rm SOG})/2$] are graphically illustrated in Fig. 2. It is evident from Table I that the splits in proton energies induced by the charge density differences are insensitive to the Coulomb exchange term. This indicates that any existing Coulomb functionals can be employed for our test of the charge density models, which will be discussed in the following subsection.

We note that the magnitude of energy splits is primarily determined by the size of Λ, but it can be significantly amplified by the shell-structure effect. As a general feature, the solution of the radial Schrödinger equation for protons is particularly sensitive to the Coulomb terms when the last occupied orbit is highly filled and has a low centrifugal barrier (low orbital angular momentum). We will refer to this phenomenon as the "weakly bound effect" throughout the remainder of this paper. This effect is the main reason behind the large energy split of approximately -500 keV for ^{32}S, which is comparable to the energy splits resulting from the use of the Slater approximation within the Skyrme HF framework, as studied in Ref. [28]. Therefore, special attention must be paid to the inclusion of this nucleus for our analyses in the following subsection. The impact on the two calcium isotopes (^{40}Ca, ^{48}Ca) is also quite significant, approximately -100 keV, while the impact for the other cases is less than 50 keV in magnitude.

B. Test of charge density models

Due to its discontinuity and nondifferentiability, the uniform distribution is not suitable for calculating the Coulomb exchange term within any existing approximations. To ensure an equal footing for evaluating the Coulomb potential for this hypothetical distribution, as well as the other charge density models listed in Sec. IV, the Coulomb exchange term will be omitted from our study in this subsection. As shown in the previous subsection, the absence of the Coulomb exchange term does not significantly affect the energy splits induced by the differences in the charge density data ($\Delta E^{\rm FB}_{\rm SOG}$), even for ^{32}S, where Λ is as large as 0.209%.

Here, we use the averaged proton energies between the FB and SOG values as a reference (denoted as $\bar{E}_R$), against which the results obtained for a given charge density model are compared. As an exception, only the FB data are used for ^{209}Bi, as a SOG analysis has not been carried out for this isotope. The proton energies evaluated with the uniform distribution, the 2pF function, and the microscopic Skyrme-HF charge density are denoted as $E_{\rm Unif}$, E_{2pF}, and E_{HF}, respectively.[1] Our results for the proton energy

[1] E_{HF} denotes the proton single-particle energies evaluated with the WS potential as a nuclear component and the charge density obtained

TABLE I. Differences in proton single-particle energies induced by discrepancies between the FB and SOG charge density data, ($\Delta E^{\rm FB}_{\rm SOG} = E_{\rm FB} - E_{\rm SOG}$). The calculation without the Coulomb exchange term is labeled as 'Direct', while those performed using the GGA and the Slater approximation are labeled as 'GGA' and 'Slater', respectively. All values are given in keV units.

Orbital	Direct	Slater	GGA	Direct	Slater	GGA	Direct	Slater	GGA	Direct	Slater	GGA	Direct	Slater	GGA
		^{16}O			^{28}Si			^{32}S			^{40}Ca			^{48}Ca	
$2p_{3/2}$													−78	−80	−71
$1f_{7/2}$										−59	−58	−53	−74	−73	−66
$1d_{3/2}$				−25	−26	−20	−452	−452	−452	−75	−72	−70	−94	−91	−86
$2s_{1/2}$				−28	−28	−20	−462	−462	−462	−82	−81	−76	−102	−100	−95
$1d_{5/2}$	2	3	0	−28	−27	−23	−460	−460	−460	−75	−73	−70	−92	−88	−84
$1p_{1/2}$	4	3	3	−36	−34	−33	−514	−514	−514	−96	−91	−91	−115	−110	−108
$1p_{3/2}$	4	4	3	−36	−34	−32	−511	−511	−511	−94	−90	−89	−112	−107	−105
$1s_{1/2}$	8	7	6	−46	−43	−42	−570	−570	−570	−118	−112	−111	−138	−130	−130
		^{54}Ni			^{205}Tl			^{206}Pb			^{208}Pb			^{209}Bi	
$2f_{5/2}$				−13	−14	−14	−16	−18		−16	−18	−19			
$2f_{7/2}$				−13	−14	−13	−17	−19	−19	−18	−19	−19			
$1h_{9/2}$				−12	−13	−12	−16	−17	−18	−16	−17	−17			
$3s_{1/2}$				−17	−17	−18	−21	−22	−23	−21	−22	−22			
$2d_{3/2}$				−16	−16	−16	−20	−21	−21	−20	−21	−21			
$1g_{7/2}$				−13	−14	−13	−18	−19	−19	−18	−18	−19			
$2d_{5/2}$				−16	−15	−16	−20	−21	−21	−20	−21	−21			
$1h_{11/2}$				−11	−11	−12	−15	−16	−17	−16	−16	−16			
$1g_{9/2}$				−12	−12	−13	−17	−17	−18	−17	−18	−18			
$1f_{5/2}$				−14	−14	−15	−20	−20	−21	−20	−20	−21			
$2p_{1/2}$	29	30	27	−18	−18	−19	−23	−23	−24	−22	−23	−24			
$2p_{3/2}$	31	32	29	−18	−18	−18	−22	−24	−24	−23	−24	−23			
$1f_{7/2}$	30	29	27	−13	−14	−14	−19	−19	−27	−23	−19	−19			
$1d_{3/2}$	37	35	34	−16	−16	−16	−22	−22	−23	−22	−22	−22			
$2s_{1/2}$	40	39	38	−20	−20	−20	−25	−26	−27	−25	−25	−27			
$1d_{5/2}$	36	34	34	−16	−15	−16	−21	−21	−22	−21	−21	−21			
$1p_{1/2}$	44	42	42	−17	−18	−18	−24	−25	−25	−23	−24	−24			
$1p_{3/2}$	43	41	41	−18	−17	−17	−23	−24	−24	−23	−23	−24			
$1s_{1/2}$	52	50	49	−20	−20	−20	−26	−27	−27	−27	−26	−27			

differences, including $\Delta E^{\rm Unif}_R = E_{\rm Unif} - \bar{E}_R$, $\Delta E^{2pF}_R = E_{2pF} - \bar{E}_R$, and $\Delta E^{HF}_R = E_{HF} - \bar{E}_R$, are given in Table II.

We note that the energy differences obtained in this subsection for all charge-density models are generally small in magnitude. In most cases, their magnitude is only a few tens of keV larger than those induced by the experimental uncertainties obtained in the previous subsection ($\Delta E^{\rm FB}_{\rm SOG}$). The values obtained for ^{32}S are somewhat larger compared to the other nuclei and are positive for all bound orbitals due to the large uncertainties in the model-independent data for charge density and an additional enhancement caused by the weakly bound effect. However, it is evident that all selected charge density models provide similar accuracy for proton single-particle energies. Notably, the microscopic Skyrme-HF calculation of charge density performs adequately, despite the various deficiencies related to isospin-symmetry breaking discussed in Ref. [14]. Generally, calculations using the uniform distribution or the 2pF function are strongly parameter-dependent. For instance, if the Coulomb radius is parametrized as $R_C \approx 1.26\,{\rm fm} \times (A-1)^{\frac{1}{3}}$, as is typical, considerably larger proton single-particle energy differences are obtained in many cases. Similarly, problems were also observed within the 2pF function. Consequently, it is necessary to constrain their parameters using relevant experimental data if these distribution functions are chosen as charge density models.

from the microscopic Skyrme-HF calculation as an input for the Coulomb potential. It should not be confused with the eigenvalues of the HF mean field.

C. Test of Coulomb functionals

The present subsection is primarily focused on compensating for the omission of the Coulomb exchange term, which is unavoidable when using the uniform distribution for the charge density. We are specifically interested in the method employed in Eq. (1), where the last proton's contribution to the Coulomb direct term is excluded. To verify this traditional idea of the self-interaction correction, it is instructive to perform an analytic analysis of its impact before discussing the numerical results.

Since the Coulomb direct term (9) is linear in charge density, it can be written as follows:

$$V_{\rm dir}\left[\rho^{Z}_{ch}\right] = V_{\rm dir}\left[\rho^{Z-1}_{ch}\right] + V_{\rm dir}\left[\rho^{1}_{ch}\right]. \tag{30}$$

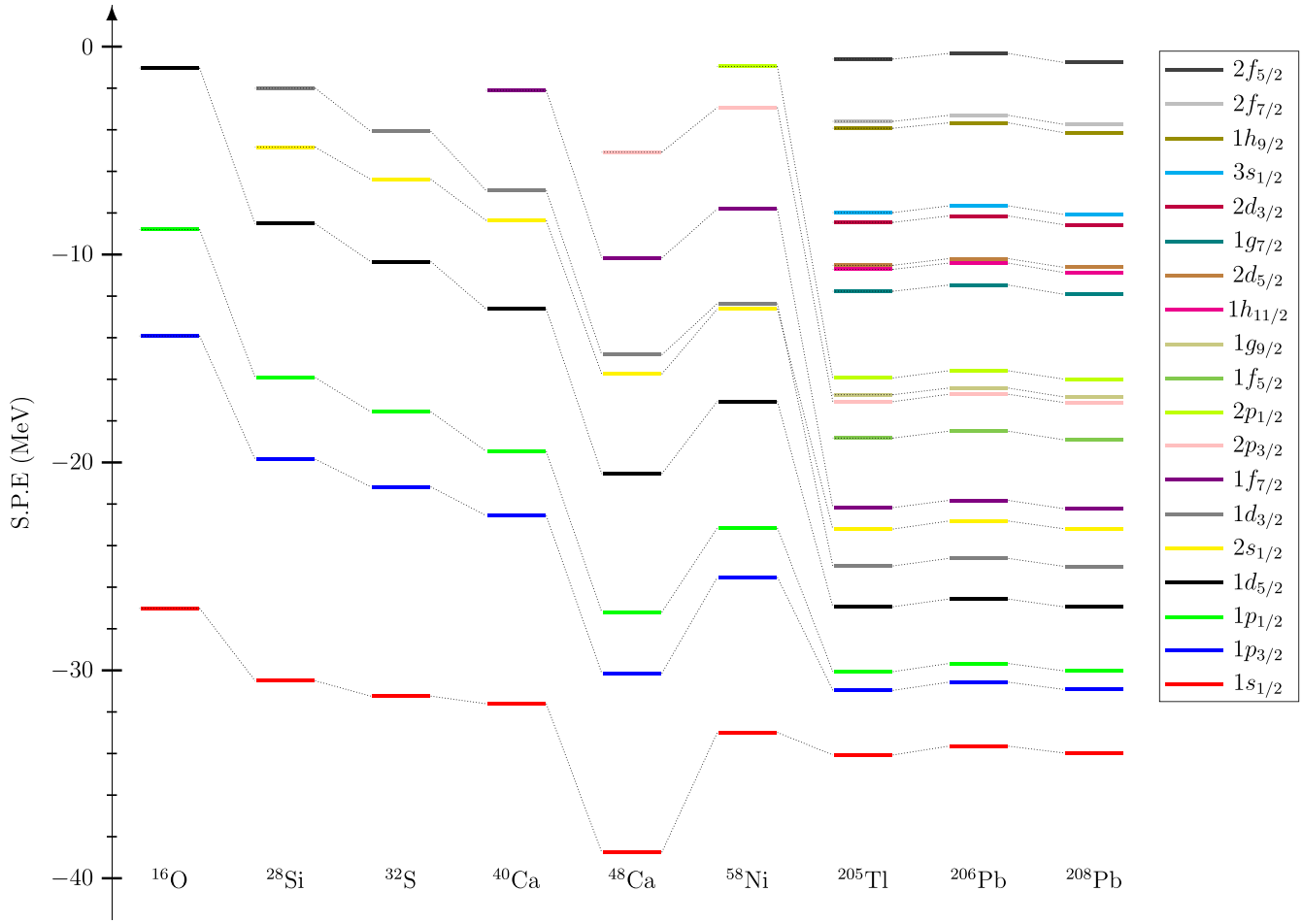

FIG. 2. Averaged proton single-particle energies between the refined FB and SOG data for the charge density. The Coulomb exchange term is evaluated with the GGA, and the spin-orbit interaction is included in the calculation.

Here, ρ_{ch}^{Z} represents the total charge density, which can be decomposed into

$$\rho_{ch}^{Z} = \rho_{ch}^{Z-1} + \rho_{ch}^{1}, \tag{31}$$

where ρ_{ch}^{1} is the contribution of the last proton and ρ_{ch}^{Z-1} is the contribution of the remaining $Z-1$ protons. To gain a better insight into the functional structure of the Coulomb direct term, we make the additional assumption that $\rho_{\rm ch}^{Z}$ and $\rho_{\rm ch}^{Z-1}$ have identical radial forms and differ from each other only by the normalization condition. Specifically, $\rho_{\rm ch}^{Z}$ is normalized to Z, whereas $\rho_{\rm ch}^{Z-1}$ is normalized to $Z-1$. This assumption is equivalent to considering that each proton has an equal contribution to the total charge density. Subsequently, the following relations can be derived:

$$\rho_{ch}^{Z-1} = \left(\frac{Z-1}{Z}\right)\rho_{ch}^{Z} = (Z-1)\rho_{ch}^{1}. \tag{32}$$

Because of the linearity, the corresponding Coulomb direct terms can be evaluated as

$$V_{\rm dir}\left[\rho_{ch}^{Z-1}\right] = \left(\frac{Z-1}{Z}\right)V_{\rm dir}\left[\rho_{ch}^{Z}\right] = (Z-1)V_{\rm dir}\left[\rho_{ch}^{1}\right]. \tag{33}$$

Based on this assumption, the self-interaction correction discussed above can be implemented simply by replacing $V_{\rm dir}[\rho_{\rm ch}^{Z}]$ with $V_{\rm dir}[\rho_{\rm ch}^{Z}] \times (Z-1)/Z$. Notably, the Coulomb potential in Eq. (1) fully satisfies these properties with $\rho_{\rm ch}^{Z}$ being the uniform distribution. An interesting observation is that the factor $(Z-1)/Z$ approaches 1 as Z approaches infinity, indicating that this correction has the greatest effect in light nuclei. We found that this replacement leads to lower proton energy levels, by about 500 keV in ^{16}O and 200 keV in ^{208}Pb, relative to the levels obtained with the pure Coulomb direct term $V_{\rm dir}[\rho_{\rm ch}^{Z}]$.

Throughout this subsection, the Coulomb functional obtained in this way will be referred to as "traditional functional". To numerically test this traditional approach, it is useful to decompose the proton energy difference for a given orbital as follows:

$$\Delta E_F^T = \Delta E_G^T + \Delta E_S^G + \Delta E_F^S, \tag{34}$$

where ΔE_F^T is defined as the single-particle energy difference between the traditional functional and the exact Fock term. On the right-hand side, ΔE_G^T, ΔE_S^G, and ΔE_F^S are, respectively, the single-particle energy differences of the traditional

TABLE II. Proton single-particle energy differences induced by the deviations of the charge-density models relative to the model-independent data. ΔE_R^{Unif}, ΔE_R^{2pF}, and ΔE_R^{HF} correspond to the uniform distribution, the 2pF function, and the Skyrme-HF calculation of charge density, respectively (see Sec. V B for a detailed description). The Coulomb exchange potential is excluded in these calculations. All values are given in keV units.

Orbital	ΔE_R^{Unif}	ΔE_R^{2pF}	ΔE_R^{HF}	ΔE_R^{Unif}	ΔE_R^{2pF}	ΔE_R^{HF}	ΔE_R^{Unif}	ΔE_R^{2pF}	ΔE_R^{HF}	ΔE_R^{Unif}	ΔE_R^{2pF}	ΔE_R^{HF}	ΔE_R^{Unif}	ΔE_R^{2pF}	ΔE_R^{HF}
		^{16}O			^{28}Si			^{32}S			^{40}Ca			^{48}Ca	
$2p_{3/2}$													−4	7	11
$1f_{7/2}$										73	6	46	113	13	13
$1d_{3/2}$				29	−18	23	667	631	693	35	8	47	85	24	5
$2s_{1/2}$				−69	−34	3	540	599	694	−72	−17	48	−6	19	8
$1d_{5/2}$	−1	−22	−10	33	−16	24	689	651	712	42	8	47	93	22	5
$1p_{1/2}$	−40	−21	−30	−38	−22	13	682	726	804	−41	3	47	34	34	−5
$1p_{3/2}$	−42	−20	−32	−32	−21	15	689	725	801	−31	4	47	43	32	−3
$1s_{1/2}$	−144	−17	−60	−159	−37	−8	618	783	894	−158	−12	48	−50	40	−10
		^{54}Ni			^{205}Tl			^{206}Pb			^{208}Pb			^{209}Bi	
$2f_{5/2}$				−70	−48	−15				−37	−72	−9	−55	−42	20
$2f_{7/2}$				−78	−50	−18	−62	−46	2	−46	−74	−11	−64	−44	18
$1h_{9/2}$				41	−46	−8	63	−39	3	84	−59	−9	58	−38	15
$3s_{1/2}$				−122	−31	−33	−120	−40	5	−109	−74	−9	−116	−33	30
$2d_{3/2}$				−83	−42	−23	−69	−42	1	−56	−72	−12	−70	−38	20
$1g_{7/2}$				20	−47	−15	41	−39	−2	59	−63	−15	35	−40	10
$2d_{5/2}$				−91	−44	−25	−78	−41	−1	−63	−73	−13	−78	−39	20
$1h_{11/2}$				59	−45	−2	81	−38	8	105	−56	−3	76	−38	18
$1g_{9/2}$				41	−46	−9	63	−39	3	84	−60	−10	57	−39	14
$1f_{5/2}$				−10	−47	−23	10	−41	−7	26	−68	−21	5	−40	9
$2p_{1/2}$	−36	−8	37	−104	−34	−32	−94	−36	0	−84	−73	−16	−92	−31	24
$2p_{3/2}$	−42	−6	36	−108	−35	−33	−99	−37	−1	−88	−73	−15	−97	−32	24
$1f_{7/2}$	90	5	49	14	−46	−16	38	−35	2	53	−64	−17	29	−40	10
$1d_{3/2}$	45	9	47	−48	−48	−30	−28	−41	−11	−16	−73	−27	−34	−42	6
$2s_{1/2}$	−52	3	40	−130	−24	−43	−128	−32	0	−122	−73	−17	−124	−25	29
$1d_{5/2}$	57	9	46	−26	−47	−26	−6	−41	−8	9	−70	−23	−11	−40	8
$1p_{1/2}$	−23	11	41	−97	−47	−40	−79	−41	−14	−70	−79	−31	−82	−40	7
$1p_{3/2}$	−9	11	43	−79	−46	−35	−62	−41	−12	−52	−77	−29	−66	−40	7
$1s_{1/2}$	−120	11	35	−152	−40	−49	−141	−39	−14	−136	−84	−32	−141	−37	11

treatment relative to GGA, GGA relative to the Slater approximation, and the Slater approximation relative to the exact Fock term. Explicitly, $\Delta E_F^T = E^T - E^F$, $\Delta E_G^T = E^T - E^G$, $\Delta E_S^G = E^G - E^S$, and $\Delta E_F^S = E^S - E^F$. As the uniform distribution is inappropriate for the evaluation of the Coulomb exchange term, the 2pF function will be selected instead for this test.

We notice that no exact treatment of the Coulomb exchange term is performed in the present work, so the data of ΔE_F^S for ^{16}O, ^{40}Ca, ^{48}Ni, and ^{208}Pb are taken from Ref. [28]. Since the mass dependence of ΔE_F^S is not strong, it is reasonable to use the values obtained for ^{40}Ca for ^{28}Si, ^{32}S, and ^{48}Ca which were not considered in Ref. [28] as they reside in the neighboring region in the nuclear chart. Similarly, we use the ΔE_F^S values obtained for ^{208}Pb for the remaining nuclei. One may argue here that ΔE_F^S may depend on the nuclear component as well as the method for solving the Schrödinger equation, or they may vary significantly when transferring from a self-consistent to a phenomenological mean field. We have checked such a dependence by examining the term ΔE_S^G, which can be evaluated within either the self-consistent mean-field framework or the phenomenological one with an externally supplied charge density. Our findings indicate that the values of ΔE_S^G obtained for ^{208}Pb within the WS potential as a nuclear component fall within the range between −1 and 19 keV (see Table III). These numbers show excellent agreement with those calculated within the self-consistent Skyrme-HF method discussed in Ref. [21]. Therefore, a similar level of agreement can be expected for the term ΔE_F^S.

Our numerical results for ΔE_F^T, ΔE_G^T, and ΔE_S^G are presented in Table III. It can be observed that in light nuclei (around $Z = 8$), negative ΔE_G^T values are obtained, indicating that the traditional self-interaction correction is stronger than the GGA exchange term. As the atomic number increases beyond $Z = 8$, ΔE_G^T gradually raises and eventually saturates around 300 keV at approximately $Z = 80$. Interestingly, the functional-driven energy differences show insensitivity to weakly bound effects, as the values obtained for ^{32}S do not differ significantly from those of neighboring nuclei, as observed in the two previous subsections. By combining these values with those of ΔE_F^S obtained from the above-cited self-consistent calculations, we find that the total energy

TABLE III. Numerical results for ΔE_G^T, ΔE_S^G, and ΔE_F^T (see Sec. V C for a detailed description). The total energy difference, ΔE_F^T, is deduced via Eq. (34) using the data for ΔE_F^S taken from Ref. [28]. All these calculations employ the 2pF function for the charge density. All values are given in keV.

Orbital	ΔE_G^T	ΔE_S^G	ΔE_F^T	ΔE_G^T	ΔE_S^G	ΔE_F^T	ΔE_G^T	ΔE_S^G	ΔE_F^T	ΔE_G^T	ΔE_S^G	ΔE_F^T	ΔE_G^T	ΔE_S^G	ΔE_F^T
		^{16}O			^{28}Si			^{32}S			^{40}Ca			^{48}Ca	
$2p_{3/2}$													22	14	−128
$1f_{7/2}$										87	−13	−84	95	−14	−77
$1d_{3/2}$				34	−11	225	70	−16	256	119	−20	301	126	−23	305
$2s_{1/2}$				−14	8	188	20	4	218	71	−3	262	79	−5	268
$1d_{5/2}$	−82	2	−254	52	−16	242	83	−20	269	125	−22	309	126	−23	309
$1p_{1/2}$	−35	−17	178	81	−24	432	106	−25	456	141	−23	493	141	−23	493
$1p_{3/2}$	−26	−21	193	84	−25	437	107	−25	460	141	−24	495	142	−25	495
$1s_{1/2}$	−5	−31	395	86	−23	561	105	−21	582	135	−17	616	137	−18	617
		^{48}Ni			^{205}Tl			^{206}Pb			^{208}Pb			^{209}Bi	
$1h_{9/2}$				278	−18	136	280	−18	138	280	−19	137	281	−18	139
$3s_{1/2}$				228	−1	366	231	−1	369	231	−2	368	232	−1	370
$2d_{3/2}$				247	−7	382	248	−6	384	249	−7	384	250	−7	385
$1g_{7/2}$				289	−18	427	290	−18	428	290	−18	428	291	−18	429
$2d_{5/2}$				244	−5	395	245	−5	396	246	−6	396	247	−6	397
$1h_{11/2}$				271	−19	393	273	−19	395	273	−19	395	275	−20	396
$1g_{9/2}$				283	−20	530	284	−19	532	284	−19	532	286	−20	533
$1f_{5/2}$				294	−17	572	295	−16	574	294	−16	573	296	−16	575
$2p_{1/2}$				263	−11	528	265	−10	531	265	−11	530	267	−11	532
$2p_{3/2}$	74	12	228	261	−10	537	262	−9	539	262	−10	538	264	−10	540
$1f_{7/2}$	148	−14	309	290	−18	625	291	−18	626	291	−18	626	292	−18	627
$1d_{3/2}$	177	−20	355	294	−14	675	296	−14	677	295	−14	676	296	−14	677
$2s_{1/2}$	133	−6	330	272	−11	643	273	−11	644	272	−11	643	274	−11	645
$1d_{5/2}$	176	−21	479	293	−15	699	295	−16	700	294	−15	700	296	−16	701
$1p_{1/2}$	189	−20	554	291	−10	750	293	−10	752	292	−10	751	294	−10	753
$1p_{3/2}$	188	−21	594	292	−12	757	294	−12	759	292	−11	758	293	−11	759
$1s_{1/2}$	183	−14	676	285	−8	797	287	−8	799	286	−7	799	287	−7	800

differences between the traditional correction and the exact treatment range from −130 to 620 keV for light nuclei, and from 136 to 800 keV for heavier nuclei. If the energy differences induced by the charge density differences are added together, a larger overall discrepancy is expected. Consequently, the expression Eq. (1) for the Coulomb potential should not be used for high precision calculations, such as the shell-model description of isospin-symmetry breaking.

VI. CONCLUSION

As part of our endeavor to improve the shell-model description of the isospin-symmetry breaking correction to superallowed $0^+ \to 0^+$ Fermi β-decay rates [5], we conducted a comprehensive and detailed investigation of the Coulomb term within the phenomenological Woods-Saxon (WS) potential. This study is divided into two main parts, each focusing on a different aspect of the Coulomb potential. The first part involves the selection of an appropriate input charge density, while the second part is dedicated to the examination of the Coulomb functional. In the first part, we performed a comparative test of the Coulomb term using various charge density models. These models include the conventional uniform distribution, the 2pF function, and the microscopic self-consistent Skyrme-Hartree-Fock (HF) calculation of the proton density, folded with the electromagnetic form factors of the proton. We observed that the differences between the proton single-particle energies obtained with these charge-density models and those resulting from the model-independent data are relatively small. In most cases, these differences are less than 100 keV. However, there is a notable exception for ^{32}S, which exhibits a high sensitivity to even small variations in the potential when the last occupied state is fully filled and lacks a centrifugal barrier. While the Coulomb-induced components in proton single-particle energies obtained using the uniform distribution and the 2pF function demonstrate remarkable accuracy, it is important to note that these quantities are generally strongly dependent on the chosen parameters. As a result, it is highly advisable to carefully constrain the parameters of these charge density models case by case by utilizing available experimental data on charge radii, as exemplified in this study. Alternatively, for more reliable and consistent results, the microscopic self-consistent Skyrme-HF calculation of charge density should be employed.

In the second part of our investigation, we thoroughly examined the traditional approach used to compensate for the exclusion of the Coulomb exchange term when the uniform distribution is chosen as a charge density model. We found that this compensation can be achieved simply by multiplying the Coulomb direct term with the factor $(Z-1)/Z$,

making it effectively a variation of the Coulomb functional. By combining our numerical results with data from the self-consistent Skyrme-HF calculation in Ref. [28], we discovered that the proton energy levels obtained with this traditional functional are underbound by 100–800 keV for nuclei with $Z \geqslant 28$, relative to those obtained with an exact treatment of the Coulomb exchange term. Conversely, the opposite pattern tends to appear in the lighter Z region, where the factor $(Z-1)/Z$ reduces significantly from unity. For example, the $1d_{5/2}$ level in ^{16}O obtained with the traditional functional is overbound by 254 keV. We were aware that making a direct comparison of single-particle energies between WS and HF calculations is not recommended, especially when examining small effects such as Coulomb repulsion. In this paper, we adopted an indirect approach for comparison, where we focused solely on the energy differences between the Slater functional and the exact Coulomb exchange. These energy differences are expected to be free from nuclear effects and were extracted from an existing Skyrme-HF calculation. By using this method, we were able to analyze the impact of the Coulomb exchange term in the context of the WS potential and its accuracy for describing nuclear structure phenomena. Furthermore, our results indicate that the functional-driven energy differences are relatively insensitive to the weakly-bound effect. Even in the case of ^{32}S, where this effect is expected to be strongest, the values obtained do not differ significantly from those of its neighboring nuclei.

In conclusion, the use of Eq. (1) for precision calculations is not recommended due to the significant discrepancies it introduces in the proton energy levels. Instead, a more reliable approach involves evaluating the Coulomb term of the Woods-Saxon potential using a realistic charge density model, such as the 2pF function or a self-consistent Skyrme-HF calculation. Additionally, a fundamental approach for the Coulomb exchange functional, such as the Slater approximation or the GGA, should be incorporated to ensure accurate results. By adopting these methods, more precise and reliable calculations can be achieved for nuclear structure studies, particularly when dealing with the isospin-symmetry breaking correction to superallowed $0^+ \to 0^+$ Fermi β-decay rates.

ACKNOWLEDGMENT

This work is supported by the National Research Foundation of Korea (NRF) grant funded by the Korea government (MSIT) (No. 2021R1A2C2094378).

[1] W. Ormand and B. Brown, Nucl. Phys. A **440**, 274 (1985).
[2] N. Auerbach, Phys. Rep. **98**, 273 (1983).
[3] Y. H. Lam, B. Blank, N. A. Smirnova, J. B. Bueb, and M. S. Antony, At. Data Nucl. Data Tables **99**, 680 (2013).
[4] O. Klochko and N. A. Smirnova, Phys. Rev. C **103**, 024316 (2021).
[5] J. C. Hardy and I. S. Towner, Phys. Rev. C **102**, 045501 (2020).
[6] N. Severijns, L. Hayen, V. De Leebeeck, S. Vanlangendonck, K. Bodek, D. Rozpedzik, and I. S. Towner, Phys. Rev. C **107**, 015502 (2023).
[7] N. Smirnova and C. Volpe, Nucl. Phys. A **714**, 441 (2003).
[8] D. Vautherin and D. M. Brink, Phys. Rev. C **5**, 626 (1972).
[9] K. Bennaceur and J. Dobaczewski, Comput. Phys. Commun. **168**, 96 (2005).
[10] S. Cwiok, J. Dudek, W. Nazarewicz, J. Skalski, and T. Werner, Comput. Phys. Commun. **46**, 379 (1987).
[11] N. Schwierz, I. Wiedenhover, and A. Volya, arXiv:0709.3525.
[12] I. S. Towner and J. C. Hardy, Phys. Rev. C **77**, 025501 (2008).
[13] L. Xayavong and N. A. Smirnova, Phys. Rev. C **97**, 024324 (2018).
[14] L. Xayavong and N. A. Smirnova, Phys. Rev. C **105**, 044308 (2022).
[15] J. Dudek, Z. Szymański, T. Werner, A. Faessler, and C. Lima, Phys. Rev. C **26**, 1712 (1982).
[16] J. Dudek, A. Majhofer, J. Skalski, T. Werner, S. Cwiok, and W. Nazarewicz, J. Phys. G **5**, 1359 (1979).
[17] A. Bohr and B. R. Mottelson, *Nuclear Structure* (World Scientific Publishing Company, Singapore, 1998).
[18] L. R. B. Elton, *Nuclear Size*, Oxford Library of the Physical Sciences (Oxford University Press, Oxford, 1961).
[19] M. W. Kirson, Nucl. Phys. A **781**, 350 (2007).
[20] B. A. Brown, S. E. Massen, and P. E. Hodgson, J. Phys. G **5**, 1655 (1979).
[21] T. Naito, X. Roca-Maza, G. Colò, and H. Liang, Phys. Rev. C **99**, 024309 (2019).
[22] J. C. Slater, Phys. Rev. **81**, 385 (1951).
[23] H. De Vries, C. De Jager, and C. De Vries, At. Data Nucl. Data Tables **36**, 495 (1987).
[24] I. Sick, Nucl. Phys. A **218**, 509 (1974).
[25] L. Xayavong, Calculs théoriques de corrections nucléaires aux taux de transitions β super-permises pour les tests du Modèle Standard, Theses, Université de Bordeaux (2016).
[26] Z.-X. Xu and C. Qi, Phys. Lett. B **724**, 247 (2013).
[27] A. M. Lane, Phys. Rev. Lett. **8**, 171 (1962).
[28] J. Skalski, Phys. Rev. C **63**, 024312 (2001).
[29] J. P. Perdew, K. Burke, and M. Ernzerhof, Phys. Rev. Lett. **77**, 3865 (1996).
[30] B. Dreher, J. Friedrich, K. Merle, H. Rothhaas, and G. Lührs, Nucl. Phys. A **235**, 219 (1974).
[31] I. S. Towner and J. C. Hardy, Phys. Rev. C **66**, 035501 (2002).
[32] C. Dover and N. Van Giai, Nucl. Phys. A **190**, 373 (1972).
[33] W. Horiuchi, Prog. Theor. Exp. Phys. **2021**, 123D01 (2021).
[34] A. B. Jones and B. A. Brown, Phys. Rev. C **90**, 067304 (2014).
[35] E. Chabanat, P. Bonche, P. Haensel, J. Meyer, and R. Schaeffer, Nucl. Phys. A **635**, 231 (1998).
[36] H. Sagawa, Nguyen Van Giai, and T. Suzuki, Phys. Lett. B **353**, 7 (1995).
[37] J. Le Bloas, M.-H. Koh, P. Quentin, L. Bonneau, and J. I. A. Ithnin, Phys. Rev. C **84**, 014310 (2011).